Human Molecular Genetics, 2000, Vol. 9, No. 7 **1131–1140**

Hailey–Hailey disease is caused by mutations in *ATP2C1* encoding a novel Ca^{2+} pump

Ralf Sudbrak[1,2], Joanna Brown[1,2], Carol Dobson-Stone[2], Simon Carter[3], Juliane Ramser[1], Jacqueline White[3], Eugene Healy[4], Manel Dissanayake[5], Marc Larrègue[6], Marc Perrussel[7], Hans Lehrach[1], Colin S. Munro[8], Tom Strachan[3], Susan Burge[9], Alain Hovnanian[2] and Anthony P. Monaco[2,+]

[1]Max-Planck-Institut für Molekulare Genetik, D-14195 Berlin, Germany, [2]The Wellcome Trust Centre for Human Genetics, University of Oxford, OX3 7BN, UK, [3]Human Genetics Unit, School of Biochemistry and Genetics, University of Newcastle Newcastle upon Tyne, NE1 7RU, UK, [4]Department of Dermatology, Southampton General Hospital, Southampton, SO16 6YD, [5]Department of Dermatology, General Hospital, Kandy, Sri Lanka, [6]Department of Dermatology, La Miletrie Hospital, Poitiers, France, [7]Cabinet Médical Wilson, Limeil-Brévannes, France, [8]Department of Dermatology, Southern General Hospital, Glasgow, G51 4TF, UK and [9]Department of Dermatology, Churchill Hospital, Oxford, OX3 7LJ, UK

Received 4 January 2000; Revised and Accepted 10 February 2000

DDBJ/EMBL/GenBank accession numbers:
human: *ATP2C1*a, AF189723; *ATP2C1b*, AF225981; *ATP2A2b*, M23114; *ATP2B2*, M97260; stMPIMG1, AJ250604; stMPIMG4, AJ250607; stMPIMG10, AJ250613; stMPIMG13, AJ250616; stMPIMG15, AJ250618; stMPIMG19, AJ250619; stMPIMG20, AJ250620; rat: SPLA, M93017; yeast: PMR1, M25488.

Hailey–Hailey disease (HHD) is an autosomal dominant skin disorder characterized by suprabasal cell separation (acantholysis) of the epidermis. Previous genetic linkage studies localized the gene to a 5 cM interval on human chromosome 3q21. After reducing the disease critical region to <1 cM, we used a positional cloning strategy to identify the gene *ATP2C1*, which is mutated in HHD. *ATP2C1* encodes a new class of P-type Ca^{2+}-transport ATPase, which is the homologue for the rat SPLA and the yeast PMR1 *medial* Golgi Ca^{2+} pumps and is related to the sarco(endo)plasmic calcium ATPase (SERCA) and plasma membrane calcium ATPase (PCMA) families of Ca^{2+} pumps. The predicted protein has the same apparent transmembrane organization and contains all of the conserved domains present in other P-type ATPases. *ATP2C1* produces two alternative splice variants of ~4.5 kb encoding predicted proteins of 903 and 923 amino acids. We identified 13 different mutations, including nonsense, frameshift insertion and deletions, splice-site mutations, and non-conservative missense mutations. This study demonstrates that defects in *ATP2C1* cause HHD and together with the recent identification of *ATP2A2* as the defective gene in Darier's disease, provide further evidence of the critical role of Ca^{2+} signaling in maintaining epidermal integrity.

INTRODUCTION

Hailey–Hailey disease (HHD; OMIM 16960) (familial benign chronic pemphigus) is a blistering dermatosis, which is inherited as an autosomal dominant trait (1–3) and usually presents around the third and fourth decades. Painful erosions, vesicopustules and scaly erythematous plaques appear at sites of friction such as the sides of the neck, the axillae, the groins and the perineum (Fig. 1a). Painful fissures (rhagades) are common in flexures and may limit mobility. Flexural disease may become hypertrophic and malodorous, but even mild disease can affect the quality of life (4). Mucosal involvement is rare, but oral, oesophageal, vaginal and conjunctival involvement have been described (5–8). The disease is characterized by recurrent exacerbations and remissions lasting months to years (1,3). Both cutaneous infections and UVB exacerbate disease (9–11). Topical corticosteroids with antibacterial agents, either local or systemic, are effective treatments in most patients (1,12).

Histologically, HHD is characterized by loss of cohesion between keratinocytes (acantholysis) with epidermal clefting or vesiculation. Widespread partial loss of the intercellular bridges between keratinocytes gives the epidermis the appearance of a 'dilapidated brick wall' (Fig. 1b). Ultrastructural studies of acantholytic cells in HHD reveal perinuclear aggregates of keratin intermediate filaments that have retracted from desmosomal plaques (13).

The histology, of HHD shows similarities to that of Darier's disease (DD), but in DD acantholysis is less pronounced, while dyskeratosis is more obvious. Keratinocytes from patients with

[+]To whom correspondence should be addressed. Tel: +44 1865 287 502; Fax: +44 1865 287 650; Email: anthony.monaco@well.ox.ac.uk

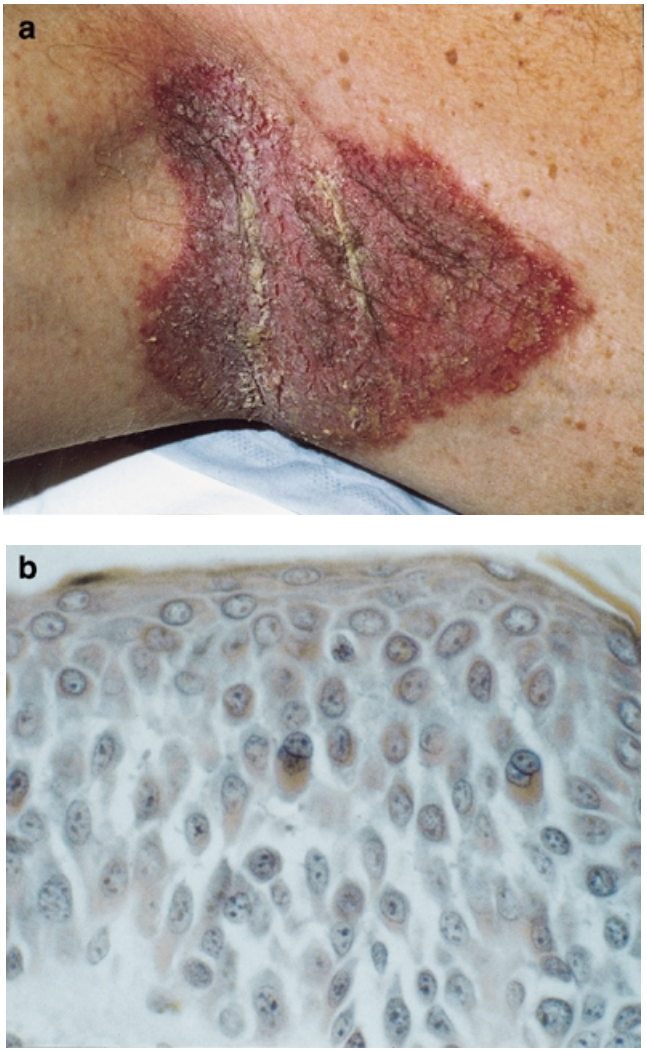

Figure 1. Clinical and histological features of HHD. (**a**) Erythematous plaque with fissures in axilla. (**b**) Widespread loss of adhesion between keratinocytes (acantholysis) (×50).

HHD dissociate spontaneously in organ culture, but acantholysis is suppressed completely by corticosteroids (14–16).

The recent identification of ATP2A2 encoding a sarco-(endo)plasmic reticulum Ca^{2+} ATPase pump as the defective gene in DD has disclosed a major role of Ca^{2+} pumps in maintaining cell–cell adhesion and normal differentiation in the epidermis (17). This discovery raised the possibility that another defect in intracellular Ca^{2+} homeostasis may underlie HHD.

HHD has been linked to chromosomal region 3q21, initially within a 14 cM interval (18). Subsequently linkage studies showed no evidence for locus heterogeneity, and the size of the critical interval was reduced further to a 5 cM region (19,20). One genomic DNA deletion in this region was detected in a single kindred (20). We analyzed additional families, refined the HHD locus to an interval of <3 cM, constructed a physical yeast artificial chromosome(YAC)/bacterial artificial chromosome(BAC)/phage 1-derived artificial chromosome (PAC) map spanning the critical genetic interval and initiated the search for candidate genes.

RESULTS

Genetic refinement of the HHD critical interval

Previous genetic mapping studies indicated that the HHD gene resided within a 5 cM interval defined by the markers D3S1589 and D3S1587. In an attempt to reduce the size of the critical region, we performed genetic analysis on HHD pedigrees with 16 polymorphic DNA markers from this interval. We obtained no evidence for genetic heterogeneity. Critical centromeric meiotic recombinations were found in one family with markers D3S1589, D3S3606 and D3S3607 (Fig. 2), which allowed us to reduce the genetic interval to a 3 cM region. To refine further the critical disease interval, we mapped genetic markers AFMa339wc5 and Mfd-2 between the cluster of markers D3S3584/D3S3606/D3S3607 and marker D3S1587. Both markers show recombination with the disease phenotype in one affected individual (Fig. 2). These results indicate that, based on recombinants, the refined HHD critical region is defined by the flanking markers Mfd-2 and D3S1587. This genetic mapping data guided further positional cloning efforts.

Physical mapping of the critical region

To develop a physical map of the region containing the HHD locus, 21 markers publicly available and located between D3S1589 and D3S1290 were used to screen the CEPH and ICRF YAC libraries. Thirty-four YACs were identified on the basis of their sequence-tagged site (STS) content. Using the YAC map and its associated markers as a starting framework, we developed a BAC/PAC contig spanning the region from marker D3S3606 to D3S1587 (Fig. 3). The identified BAC/PAC clones were tested for the presence of expressed sequence tags (ESTs) and STSs mapped in the region. Additional markers developed from insert ends of strategically selected BAC/PAC clones were also used for BAC/PAC library screening to isolate new clones. This effort resulted in the construction of a bacterial clone contig between D3S3606 and D3S1587 with two gaps in clone representation (Fig. 3). The map consists of 45 ESTs, nine STSs generated from insert ends of BAC and PAC clones, four further STSs and six polymorphic markers. Mapping of these markers on the contig revealed that AFMa339wc5 was centromeric to Mfd-2, thus defining the HHD critical region between markers Mfd-2 and D3S1587 (Fig. 3).

Isolation and characterization of cDNA

The identification of *ATP2A2* as the defective gene in DD guided our attention to Ca^{2+}-ATPases as candidates for HHD. The EST stSG2295, which is located in the HHD critical interval, shows similarity to calcium transport ATPases. Searching the non-redundant database by blastN with EST stSG2295 identified the partial human mRNA AJ010953 and the alternatively spliced rat homologues (M93017, M93018). A blast search with M93017 against dbEST identified a single human EST AA320285 located upstream of the 5′ end of AJ010953. Based on the sequence of EST AA320285, PCR primers were designed to screen a keratinocyte cDNA library. We identified clones 55B17 (from keratinocyte cDNA library RZPD550) and 56D7 (from keratinocyte cDNA library

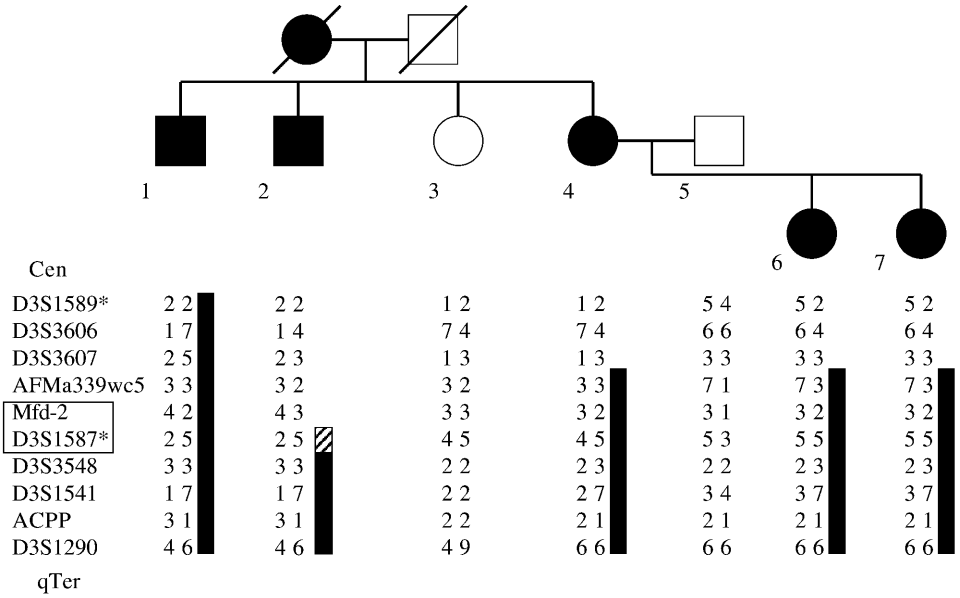

Figure 2. Haplotype analysis of the HHD family showing critical centromeric recombinants. The alleles shown in black are those associated with HHD. Non-informative markers are cross hatched. Asterisks denote the markers flanking the previously described HHD region. A meiotic recombination event in individual 2 locates the HHD distal to Mfd-2. The new critical interval flanked by Mfd-2 and D3S1587 is boxed.

RZPD558), which contain together the full length cDNA (AF189723). Sequence analysis of the isolated cDNA revealed a predicted open reading frame (ORF) of 2712 bp encoding a 903 amino acid protein. The ORF is preceded by 202 bp of 5′ untranslated sequence. The sequence around the putative ATG translation start site (ACAATGA) contains the critical –3 purine of a Kozak consensus sequence (21).

By searching the blast dbEST database and sequencing IMAGE clones, alternate polyadenylation was detected. In the 3′ untranslated sequence five putative polyadenylation signals (AATAAA) starting at positions 3316, 3719, 3899, 4650 and 4690 are present. Poly(A) tracts starting at positions 4671 and 4712 were identified. The two isolated keratinocyte cDNA clones show an additional alternate polyadenylation at position 3556 using the AGTAAA sequence as a polyadenylation signal. This cDNA sequence shows at least three different sized 3′ ends corresponding to UniGene clusters Hs.47168 (EST stSG21646) and Hs.106778. In addition, a splice variant showing an alternative 3′ coding and untranslated sequence could be identified by sequence data base analysis. The point of divergence between the two isoforms occurred after codon 892. The alternatively spliced isoform (*ATP2C1b*) revealed a predicted ORF of 2772 bp encoding a protein of 923 amino acids. Amino acid 893 is in both cases Val, but is encoded by different codons [isoform a (*ATP2C1a)*: GTT; isoform b: GTC]. Isoform b terminates with a 464 bp 3′ untranslated sequence containing UniGene cluster Hs.48119 (ESTs stSG2295 and stSG42328). Northern blot hybridization of total keratinocyte RNA using a probe specific for the 3′UTR of *ATP2C1* showed a 4.5 kb transcript highly expressed (data not shown).

Genomic organization of *ATP2C1*

The EST stSG2295 mapped onto BAC clones RG139I22, RG356K14 and RG148L10. To obtain the exon–intron organization of the *ATP2C1* gene we performed vectorette-PCR with primers generated from the cDNA sequence. During this procedure it became obvious that BAC RG356K14 contains only the 3′ end of the *ATP2C1* gene, whereas clone RG139I22 harbors the complete gene. By sequencing vectorette-PCR products we obtained 30 kb of novel sequence and were able to predict all exon–intron boundaries of *ATP2C1* based on sequence comparison between the cDNA and the vectorette-PCR product sequences (Table 1). The ORFs are distributed across 26 and 27 exons, respectively, starting in exon 2; these range in size from 36 to 172 bp (excluding the 3′ exons). Exon 1 is highly GC-rich (76.3 %), contains 20 CG dinucleotides and forms with the adjacent sequence a putative 1 kb CpG island. The GT dinucleotide at position 2879–2880 of the cDNA of isoform a is used as a cryptic donor splice site in isoform b eliminating the last 33 bp of the predicted ORF and the complete 3′ untranslated sequence of exon 27. This sequence is replaced by exon 28 in isoform b.

In conclusion, we identified *ATP2C1*, which is present as two splice variants with at least four different 3′ untranslated termini. Analysis of 30 kb sequence obtained by sequencing vectorette-PCR products showed that at least four UniGene clusters are assigned to this gene.

Computational analysis of *ATP2C1* and its encoded protein

The predicted protein contains all of the conserved domains commonly found in P-type ion-transport ATPases. The seven amino acid motif DKTGT-[LIVMS]-[TIS] (motif no. PS00154 in the PROSITE (22) database of protein motifs), which classifies a protein as a P-type ATPase, next to the aspartate, which is phosphorylated during the reaction cycle, is found in the sequence DKTGTLT (position 334–340) in the protein encoded by ATP2C1. The enzyme also contains two sequences around the reactive Lys-464 (23) and Asp-628 (24), which are thought to form part of the ATP binding site. All three amino

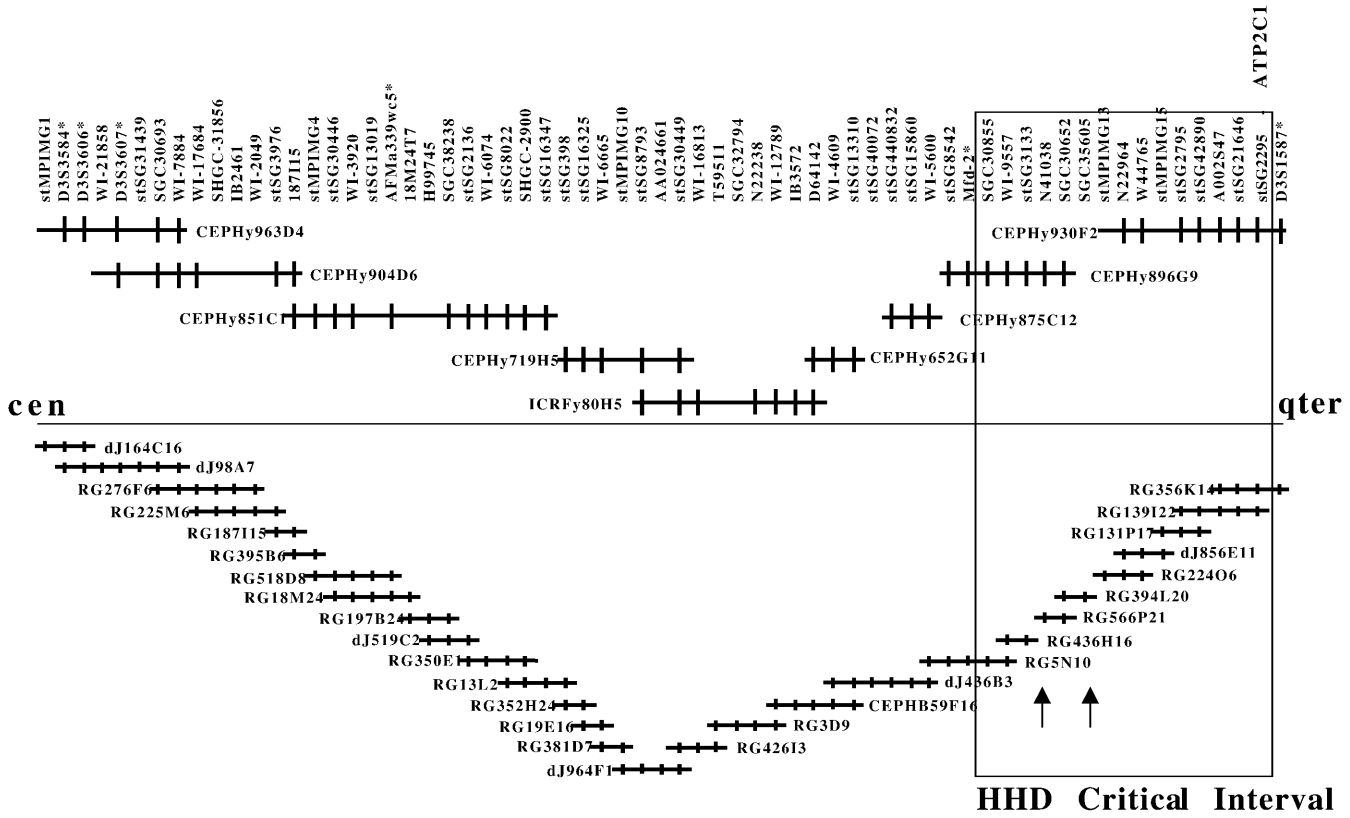

Figure 3. Physical map of the HHD region in 3q21. Marker positions are indicated by vertical bars. YACs are shown above the horizontal line, PACs and BACs are below. The two vertical arrows point to the gaps in the PAC/BAC contig. Asterisks denote polymorphic markers. The HHD critical region delineated by new centromeric recombinants is boxed. The position of *ATP2C1* is indicated above EST stSG2295.

acid residues have been reported to be essential for the activity of ion-transporting ATPases.

Similarity comparisons demonstrate that the amino acid sequence encoded by *ATP2C1* most closely resembles those of rat SPLA Ca^{2+} pump (25), the yeast secretory pathway PMR1 pump (26) and the sarco(endo)plasmic calcium ATP-ase (SERCA) (27) and plasma membrane calcium ATP-ase (PMCA) classes of mammalian Ca^{2+} pumps (28). A multiple-sequence alignment of the predicted amino acid sequence of the product encoded by *ATP2C1* with SPLA, PMR1, SERCA2 and PMCA2 (Fig. 4) reveals a high number of conserved positions including sequences around Asp-334, Lys-464 and Asp-628. The protein has the four major hydrophobic domains in the N-terminal half of the protein and the six hydrophobic domains in the C-terminal half that correspond to the known transmembrane domains of the other transport ATPases. The highest degree of similarity occurs between the predicted transmembrane domains 2 and 3, and between the transmembrane domains 4 and 5. By analogy with other P-type ATPases, these conserved regions are predicted to contain the cytoplasmic domains involved in ATP binding, phosphorylation and conformational changes of the enzyme. Thus, the predicted protein has the same apparent transmembrane organization and comprises all of the conserved domains characteristic of the P-type ATPases. In addition, the protein contains six potential Ca^{2+} binding sites, three of which (E292, N722 and D726) are located in transmembrane domains 4 and 6, and are conserved among all five pumps (29), while three other sites (A697, M725 and D803) are located in transmembrane domains 5, 6 and 8, respectively, and are conserved among ATP2C1, SPLA and PMR1 (Fig. 4).

In pairwise comparisons, the predicted protein exhibits 97% amino acid identity to rat SPLA, 49% identity to yeast PMR1, 37% identity to human SERCA2 and 31% identity to human PMCA2. It should be noted that both the rat SPLA and yeast PMR1 pumps are *medial*-Golgi Ca^{2+} pumps that exhibit 50% amino acid identity, while SERCA2 and PMCA2, which are members of two different classes of human Ca^{2+} pumps, share only 29% amino acid identity. On the basis of these comparisons, it seems likely that the protein encoded by *ATP2C1* represents a third class of human Ca^{2+} ATPase pump, which is the human homologue for the rat SPLA and the yeast PMR1 pump.

ATP2C1 mutations in HHD families

ATP2C1 cDNA was amplified from lymphoblasts from seven patients from different HHD families and was screened for mutations by Conformation Sensitive Gel Electrophoresis (CSGE) analysis. The entire coding sequence and flanking intron boundaries were amplified from genomic DNA in nine additional HHD patients from unrelated families. Bands of abnormal electrophoretic mobility were seen in 14 patients and sequencing of these PCR products revealed 13 different mutations (Table 2, Fig. 5). No mutation was found in two families

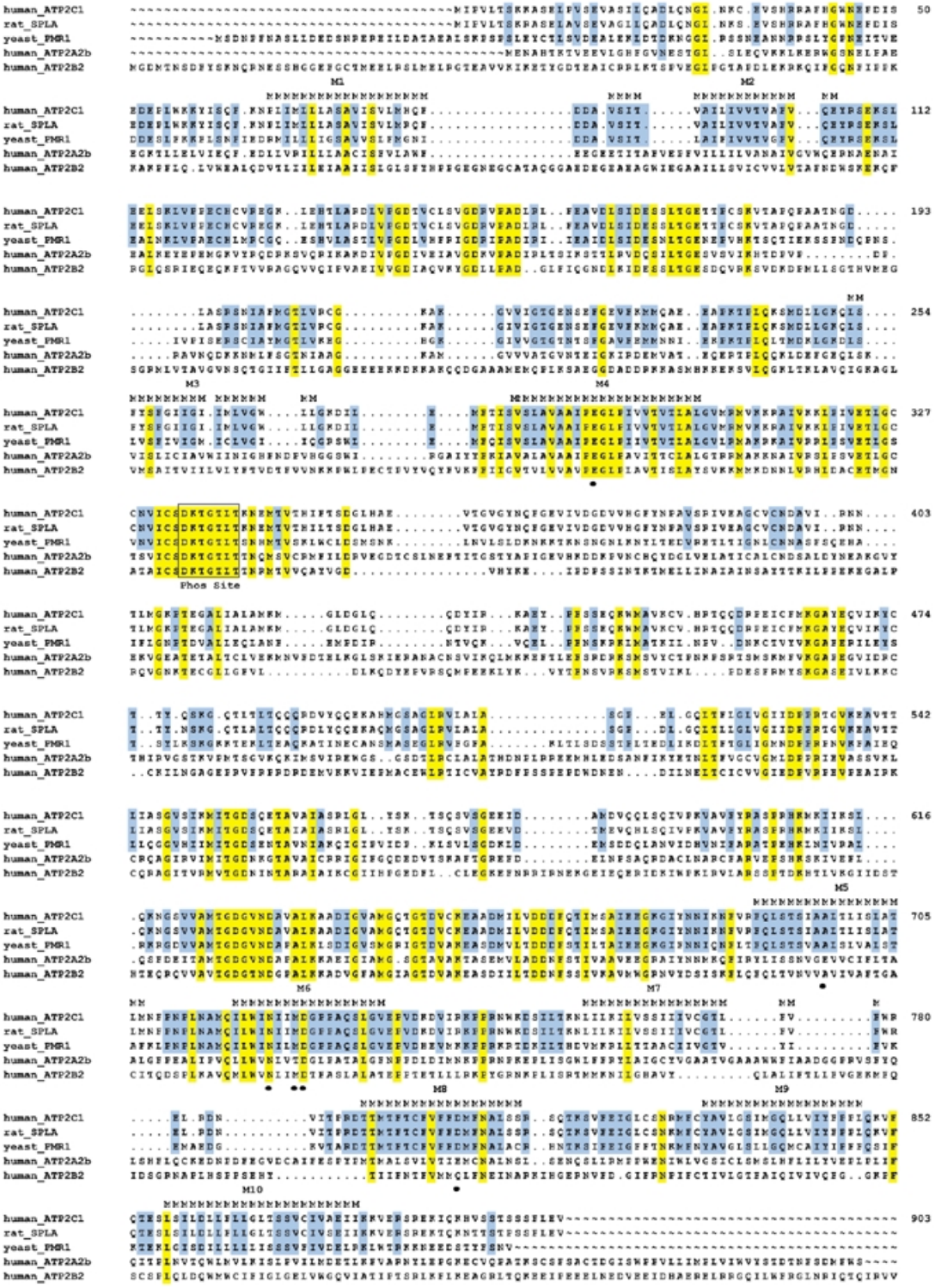

Figure 4. Amino-acid sequence alignment of the protein encoded by human *ATP2C1* with *medial*-Golgi Ca^{2+} pumps (rat SPLA, yeast PMR1), human sarco(endo)plasmic Ca^{2+}-ATPase pump encoded by *ATP2A2* and human plasma membrane Ca^{2+}-ATPase pump encoded by *ATP2B2*. Identical residues in all family members are highlighted in yellow, and those conserved in Golgi-pumps only are shown in blue. Hydrophobic regions which may represent transmembrane domains are represented by a stretch of M and are numbered (M1 to M10). The potential phosphorylation domain (Phos site) is boxed. Putative Ca^{2+} binding sites (E292, A697, N722, M725, D726 and D803) are indicated by dots. Amino acid numbers of *ATP2C1* are shown on the right.

with typical HHD after direct sequencing of the entire coding region of ATP2C1 cDNA. Four substitutions resulted in premature termination codons (PTCs) (R39X, Q427X, S546X, Q849X). Two deletions (2180delG and 2326delTTTG) created

Table 1. *ATP2C1* coding region: intron–exon organization

Exon/ intron	Exon length (bp)	Starting position in cDNA	Acceptor splice site[a]	Donor splice site[a]
1	172	1		GGCTTTGGgtgggtaccagtatta
2	111	173	tggttttacttcctagGTTGCACG	TTCTCCAAgtaagtggttagtggg
3	117	284	gtataaactctaatagGCTGATCT	TTTCTCAGgtgagatacttttact
4	90	401	aagtttttactttcagTTTAAAAA	TCACTGTGgtaagaaaaaaataca
5	36	491	tgtttcttttgtttagGCAATACT	TTGTTCAGgtaagtactctatttt
6	62	527	ttttttgtttgaatagGAATATCG	TGCCATTGgtatgatccttttttt
7	109	589	ctatttcgtgttacagTGTGCGTG	TGTTTGAGgtaaatttgggatctg
8	156	698	ctttatgttccctaagGCTGTGGA	AAGCAAAGgtaaatttttttcctg
9	69	854	ctgtttttccccttagGGTGTTGT	CAGAAGAGgtgagtacttaatatg
10	76	923	tcttcaatttatcaagGCACCAAA	TATAATAGgtaagagaagagtgag
11	67	999	tttaattatctttcagGAATCATC	AGTGTAAGgtaagtctcaatactt
12	125	1066	tatatgttggttatagTTTGGCTG	AACTCTGGgtaagtctgtgttaag
13	98	1191	tgatttaattctttagGCTGCTGT	ATGCTGAGgtactctataggtttt
14	96	1289	actttgtgatctttagGTTACTGG	TTGTTGAGgtaaatatttttttt
15	90	1385	tgtgtatttttcttagGCGGGCTG	CAATGAAGgtacgtacctaaattt
16	105	1475	tctttgtgccatatagATGGGTCT	CACAGCAGgtatccatctgtttaa
17	157	1580	tacattttcttcttagGACAGACC	ACTCAGAGgtaaggctatttcagc
18	171	1737	tttattatttcctaagTTCTTGCT	TGCAATCGgtataactagactgct
19	98	1908	ctctcatttgctttagCCAGTCGT	TACCAAAGgtaggcctaaactaaa
20	51	2006	tcttgtattttaacagGTTGCAGT	TTATTAAGgtgagtgtgtaagaat
21	167	2057	ctctgctccactctagTCGCTACA	ACCATAATgtaagctttgtttcag
22	69	2224	atttttaaatttcagGTCTGCAA	CTGAGCACgtaagtttgcaagaaa
23	117	2293	ctctctttttcaacagGAGTATAG	GCTCAGAGgtacgagtttttaat
24	148	2410	tctgtttgtttttaagCCTTGGAG	GGCGTGAGgtatattcactggcca
25	96	2558	tattgcctcttgacagCTACGAGA	GATCCCAGgtatgtttaggtgaac
26	142	2654	tctgctctgccaacagACCAAGTC	CATACTGGgtaaagaaaacgttat
27a	1936	2796	ttattttctcttgcagATCTGTTG	
27b	95	2796	ttattttctcttgcagATCTGTTG	AGAAGCATGTCTGGCTCTGGGAGA[b]
28	561	2891	gtgcttaccgagttagGTCTGGCT	

[a]The exonic and intronic sequences are indicated in upper case and lower case letters, respectively.
[b]This sequence, located within exon 27, is spliced at a GT cryptic donor splice site (underlined) to generate *ATP2C1b* isoform by joining exon 28 to the first 95 nucleotides of exon 27. *ATP2C1a* isoform contains the entire exon 27 and no exon 28 sequence.

shifts in the reading frame and resulted in PTCs. Three splice site mutations occurred at the guanine of the conserved AG dinucleotide in the acceptor splice site of introns 11, 18 and 26. These mutations probably alter splicing of exons 12, 19 and 27, respectively, although the precise consequence is unknown as RNA was not available for these patients. Three missense mutations were identified, P185L, C328Y and T554I, which are located in the predicted cytoplasmic β-strand, phosphorylation and nucleotide binding domains of the molecule, respectively. T554I was present in two families not known to be related (Table 2). Each of these mutations result in non-conservative amino acid substitutions at positions conserved with the rat SPLA sequence and the human *ATP2A2b* sequence (Fig. 4). None of these mutations were detected in 50 control individuals (100 chromosomes), indicating that these mutations are not likely to be neutral polymorphisms. Finally, a guanine deletion followed by a large insertion of ~23 adenines and a thymine was identified in family NC2. Sequencing of 12 subclones of this region revealed the number of adenines inserted to vary from 19 to 26, making the precise consequence of this mutation difficult to predict.

During the search for mutations, a G2550A substitution in exon 26 of *ATP2C1* was found. This substitution does not change the amino acid coding and does not alter transcript size in the relevant patients, so is presumed to be a neutral polymorphism. Probands from families OX8, FR1, NC1, OX6 and FR2 were found to be heterozygous for this polymorphism; the

Table 2. *ATP2C1* mutations in patients with HHD

Family	Location	Mutation[a,b]	Nucleotide change[c]	Mutation type	Verification method
NC2	exon 2	28delGins~24	CAAAAAAAGC→CAAAAAAA...ATC	? large insertion[d]	4% agarose gel
OX5	exon 3	R39X	115C→T	nonsense	*Cac*8I, *Hph*I
OX3	exon 8	P185L	554C→T	missense	*Sap*I
FR2	intron 11	852-1G→A	cagGAA→caaGAA	splice site	*Psi*I
FR3	exon 13	C328Y	983G→A	missense	DHPLC
NC1	exon 16	Q427X	1279C→T	nonsense	*Mse*I
SL1	exon 18	S546X	1637C→G	nonsense	*Mnl*I
OX1	exon 18	T554I	1661C→T	missense	*Bsr*I
OX2	exon 18	T554I	1661C→T	missense	*Bsr*I
OX6	intron 18	1694-1G→A	tagCCA→taaCCA	splice site	*Mse*I
FR1	exon 23	2180delG	TGGACC→TGACC	frameshift (PTC+8 aa)[e]	*Ava*II
OX7	exon 24	2326delTTTG	ATTTGTTTGTCT→ATTTGTCT	frameshift (PTC+9 aa)	*Tth*111I
OX4	exon 26	Q849X	2545C→T	nonsense	*Eco*57I
SL2	intron 26	2582-1delG	cagATC→caATC	splice site	*Bgl*II

[a]Amino acids are numbered according to the predicted ATP2C1 peptide sequence.
[b]Nucleotides are numbered according to the cDNA sequence, with the adenosine of the initiation codon assigned position 1.
[c]Intronic bases are denoted in lower case, exonic bases in upper case; bases altered by the mutation are underlined.
[d]As the precise number of bases inserted in this mutation was not determined, it is not known whether a shift in the reading frame is incurred.
[e]The downstream amino-acid position of premature termination codons is indicated in parentheses after the relevant frameshift mutation.

remaining probands were all homozygous for the guanine at this site.

DISCUSSION

We used a positional cloning strategy to identify *ATP2C1*, the defective gene in HHD. We refined the genetic interval to <1 cM by identifying critical meiotic recombinants, developed a physical map of the region and identified a new Ca^{2+}-ATPase using a combination of bioinformatic analysis and keratinocyte cDNA library screening. We identified 13 mutations predicted to alter the *ATP2C1* gene product in affected members of 14 HHD families, thus demonstrating that *ATP2C1* is the gene involved in HHD.

The protein is a new member of the P-type ion-transport ATPases, which is highly expressed in keratinocytes. Multiple sequence alignment suggests that it is the human homologue for the rat SPLA and the yeast PMR1 Ca^{2+} pumps, both of which are *medial*-Golgi pumps (25,26,30). The conservation of functional domains that are common to other Ca^{2+}-ATPases suggests that ATP2C1 actively transports Ca^{2+} from the cytosol to the lumen of the Golgi apparatus. ATP2C1 would thus play an important role in maintaining Ca^{2+} concentrations within compartments of the Golgi apparatus. Our results provide convincing evidence that disruption of *ATP2C1* causes HHD.

Six of these mutations are predicted to prevent expression of the corresponding protein to produce a truncated or absent protein. In three families, the mutation alters a predicted splice site. Three other mutations are predicted to cause missense changes that are unlikely to be polymorphisms as they were not found in 50 controls. These mutations are located in predicted cytoplasmic domains of the molecule thought to be involved in catalytic activities of P-type ATPases. Mutation P185L occurred in the β-strand domain at a position that is conserved between ATP2C1, rat SPLA and human ATP2A2. Mutation C328Y is located in the phosphorylation domain, five amino acids upstream of the conserved phosphorylation sequence DKTGT, which is found in all P-type ATPases. Mutation T554I is located in the nucleotide binding site of the molecule and occurs at a position that is conserved among the three types of Ca^{2+} pumps (Fig. 4). This mutation is identical in two families (OX1 and OX2) of British origin, and studies are under way to determine if this reflects a founder effect. Although the precise consequence of these missense mutations could not be predicted, the expected effect of the other mutations is the absence of production of the mutated polypeptide. These findings support a mechanism through haploinsufficiency, suggesting that epidermal cells are sensitive to *ATP2C1* gene dosage. Interestingly, a similar disease mechanism has been proposed for the majority of *ATP2A2* mutations found in patients with DD (17,31,32). Although both diseases show acantholysis of epidermal cells and may show some clinical overlap, erosions and blistering are prominent features in HHD while dyskeratosis predominates in patients with DD. Thus, dysfunction of *ATP2A2* and *ATP2C1* appears to have different effects on cell–cell adhesion and differentiation of the epidermis.

Extracellular calcium plays a crucial role in regulating differentiation and adhesion of cultured keratinocytes (33,34).

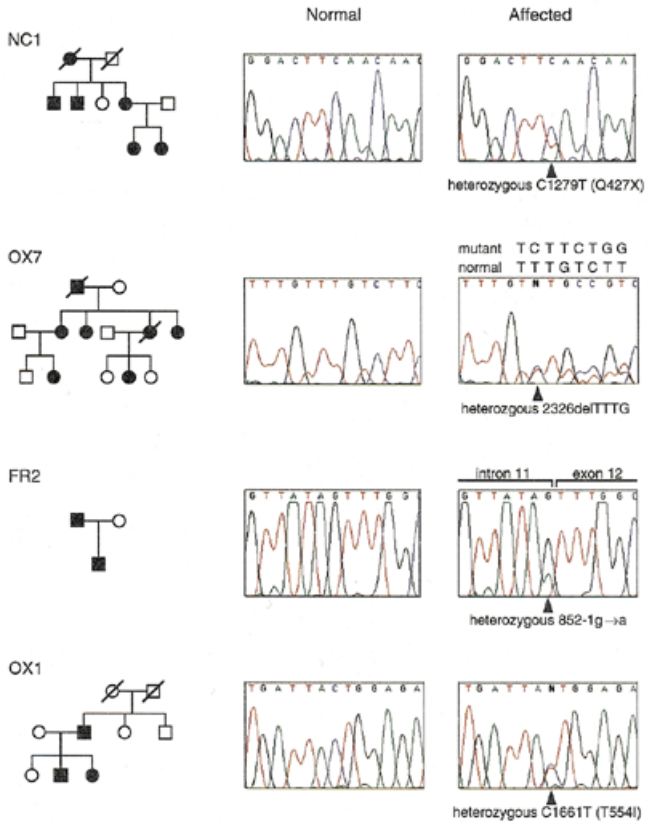

Figure 5. Identification of *ATP2C1* mutations in patients with HHD. The pedigrees of families NC1, OX7, FR2 and OX1 are shown alongside sequences generated by direct sequencing of genomic DNA amplicons from (left) a control individual and (right) the relevant proband. The sequences illustrate respectively the nonsense, frameshift, splice site and missense mutations found in these families. Affected indivduals are indicated in the pedigree by filled symbols, unaffected by open symbols. Arrowheads indicate the position of the mutation in the proband sequence. For the OX7 proband, the mutant and normal alleles whose superimposition is caused by the 4 bp deletion are displayed above the sequence.

Low levels of Ca^{2+} induce their proliferation while physiological levels of extracellular Ca^{2+} induce cell-to-cell adhesion and keratinocyte differentiation through the expression of many markers associated with formation of a cornified layer. The mechanisms that are implicated are unclear, but probably involve changes in intracellular calcium levels. In normal human epidermis, the presence of an increasing Ca^{2+} gradient from the basal cells to the upper granular cells (35) where several Ca^{2+}-mediated differentiation markers are expressed, strongly suggests that Ca^{2+} also plays an important role *in vivo*. Our results, together with the recent identification of *ATP2A2* mutations in DD, indicate that Ca^{2+} stores in the endoplasmic reticulum and the Golgi apparatus play a key role in epidermal differentiation and/or adhesion. Reduced ATP2C1 activity is thought to decrease intraluminal Ca^{2+} concentrations in the Golgi and may also have an effect on cytosolic Ca^{2+} concentration. Among processes carried out in the lumen of the Golgi, post-translational modifications such as glycosylation, folding, trafficking and/or sorting of key molecules involved in cell-to-cell adhesion may be altered (36,37). By analogy with Pmr1-defective yeast, alterations in the secretory pathway and/or the clearance of misfolded proteins could also be involved (38,39). It is also possible that dysfunction of the ATP2C1 pump could have an effect on cytosolic Ca^{2+} concentrations, thus impairing intracellular signaling pathways that regulate cell adhesion through the phosphorylation of target proteins and/or the regulation of gene transcription (40–42).

Further studies on the precise effects of *ATP2C1* mutations on cell-to-cell adhesion and differentiation through the identification of target molecules should improve our understanding of the Ca^{2+}-dependent biological pathway involved in the disease. This may help in the development of specific therapeutic approaches aiming to restore normal Ca^{2+} homeostasis in the epidermis of these patients.

MATERIALS AND METHODS

Families

A total of 149 individuals, including 69 affected members from 15 families were included in this study. Diagnosis was established by a dermatologist, on the basis of physical examination and was confirmed by histological examination of a skin biopsy in at least one member of each family. Peripheral blood was collected in EDTA for DNA isolation, and in acid citrate dextrose for the establishment of Epstein–Barr virus-transformed lymphocytes by standard methods. In addition, genomic DNA was extracted from buccal smears. Blood samples, buccal smears and skin biopsies were obtained after patients had given informed consent.

Genotyping

Sixteen polymorphic DNA markers (D3S1589, AFM203wc10, D3S3584, D3S3606, D3S3607, AFMa339wc5, Mfd-2, D3S1587, D3S3548, D3S3514, D3S1292, D3S1596, D3S1273, D3S1290, D3S1541, ACPP) between D3S1589 and D3S1290 were used in this study. Forward PCR primers were labelled with either 6-FAM, HEX or TET phosphoramidite. Microsatellite analyses were performed by PCR amplification of 40 ng of genomic DNA in a 25 µl reaction containing 10 pmol each of the forward and reverse primer, 200 µM dNTPs, 1× reaction buffer (1.5 mM $MgCl_2$, 45 mM Tris pH 8.8, 11 mM $[NH4]SO_4$ pH 8.8, 6.7 mM β-mercaptoethanol and 4.5 µM EDTA), and 0.7 U of AmpliTaq DNA polymerase (Perkin Elmer Applied Biosystems, Foster City, CA). Amplification was performed with an initial denaturation at 94°C for 5 min and 35 cycles at 94°C for 30 s, at either 50, 55 or 58°C for 30 s, and at 72°C for 30 s, in an MJ Research PTC-225 thermal cycler. Products were mixed with an equal amount of formamide buffer, and run on a 373A sequencer (Applied Biosystems), followed by analysis with GENESCAN (version 2.0.2) and GENOTYPER (version 1.1) software to derive allele sizes.

Clone isolation

YACs were identified from total human genomic CEPH Mega-YAC and ICRF YAC libraries. PACs were identified from the RPCI1, 3–5 library created by P. de Jong, and BACs were identified either from the Research Genetics human BAC library or from the CEPH BAC library. Clones were identified by PCR-based screening of DNA pools with publicly available STSs. After isolation, individual clones were tested by colony PCR to establish their STS content. As the clone contig

assembly proceeded, clones were selected for the generation of insert end-specific STSs by vectorette-PCR.

Development of YAC-, BAC- and PAC-insert end-specific STSs

YAC-, BAC- and PAC-end sequences were isolated by established vectorette-mediated PCR techniques (43,44). DNA was digested with *Rsa*I, *Alu*I, *Hae*III, *Pvu*II, *Hpa*I, *Eco*RV and *Sca*I and was blunt-end ligated to double-stranded vectorette. The vectorette libraries were amplified with both the vectorette primer and a primer for either the right or the left arm of pYAC4, for YAC insert end recovery, and were amplified with either T7 or Sp6 primers for isolation of BAC and PAC insert ends. End fragments were sequenced, and PCR primers were designed.

Analysis of BAC and PAC clones

Pulsed-field gel electrophoresis separation of *Not*I-digested BAC and PAC clones was used to determine the insert size, as well as the presence of internal *Not*I restriction sites. The digested samples were run on 1% agarose gels at 6 V/cm for 20 h, at an initial pulse time of 4 s and a final pulse time of 20 s, with a CHEF DRII (Bio-Rad, Hercules, CA) apparatus.

FISH analysis

Clones were tested by FISH analysis for chromosomal location and chimerism. One microgram of DNA was biotinylated by nick translation with the Bionick Labelling System (Life Technologies, Rockville, MD) and was processed by standard techniques.

Mutation analysis

Total RNA was extracted from immortalized lymphocyte cell lines using Trizol (Life Technologies). First strand cDNA was synthesized from RNA (5 µg) with Superscript reverse transcriptase (Life Technologies) and random hexamer primers (Pharmacia Biotech., Uppsala, Sweden). The entire coding sequence of *ATP2C1* cDNA was amplified using overlapping sets of primers (sequence available on request). PCRs were carried out with standard reaction mixes containing 2.5 mM $MgCl_2$. After an initial denaturation step at 94°C for 15 min, 35 cycles of amplification consisting of 30 s at 94°C, 30 s at 58°C and 30 s at 72°C were performed. RT–PCR products were run on 3% agarose gels for detection of splicing abnormalities prior to mutation screening by CSGE. For CSGE analysis, the formation of heteroduplexes was enhanced by heating RT–PCR products to 98°C for 5 min, followed by 68°C for 1 h. Samples (5 µg) were loaded onto a gel containing 10% polyacrylamide, 15% formamide, 10% ethylene glycol and 0.5× glycerol-tolerant buffer (USB) and were subjected to electrophoresis at 500 V for 16 h. The gel was stained with ethidium bromide and visualized under an ultraviolet transilluminator. RT–PCR fragments showing aberrant migration patterns or extra bands were sequenced in forward and reverse orientations. PCR products showing aberrant migration patterns or extra bands were purified using a QIAquick PCR purification kit (Qiagen). These were then directly sequenced in both directions by means of the BigDye Terminator Cycle Sequencing Ready Reaction kit (PE-Applied Biosystems) and were run on an ABI 377 DNA Sequencer (PE-Applied Biosystems). Where RNA was not available, all 26 translated exons plus flanking splice sites were amplified from genomic DNA (primer sequences available on request), analysed by CSGE and sequenced as described above. The different-sized products resulting from amplification of exon 2 in the proband of family NC2 were subcloned into pGEM-T vector (Promega Corp., Madison, WI) and multiple subclones were sequenced. The presence of the mutations was verified by restriction digestion or denaturing high-performance liquid chromatography.

ACKNOWLEDGEMENTS

We are grateful to the patients and their families. This work was supported by The Wellcome Trust. R.S. was supported by the EU HCMP fellowship CT940570 and the Deutsches Human Genome Project (DHGP/BMBF Grant 01KW9608). A.H. held a DEBRA UK fellowship and is a Wellcome Trust Senior Clinical Fellow. A.P.M. is a Wellcome Principal Research Fellow. The authors would like to thank the DHGP for providing genomic and cDNA clones.

NOTE ADDED IN PROOF

Whilst this manuscript was under review, Z. Hu *et al.* reported the identification of *ATP2C1* as the HHD gene [mutations in *ATP2C1*, encoding a calcium pump, cause Hailey–Hailey disease, *Nature Genet.*, (2000) **24**, 61–65]. In this article, the coding sequence of *ATP2C1* starts 16 amino acids upstream of the sequence which we describe. Genomic sequencing showed that these two isoforms result from alternative splicing of an additional exon located between exons 1 and 2 (data not shown). Alternative splicing also accounts for *ATP2C1b* described by Z. Hu *et al.*, which results from joining exon 26 to exon 28.

REFERENCES

1. Burge, S.M. (1992) Hailey–Hailey disease: The clinical features, response to treatment and prognosis. *Br. J. Dermatol.*, **126**, 275–282.
2. Richard, G., Linse, R., Hadlich, J. and Schubert, H. (1990) Zur genetik des pemphigus benignus chronicus familiaris Hailey–Hailey. *Dermatol. Monatsschr.*, **176**, 673–681.
3. Palmer, D. and Perry, H. (1962) Benign familial chronic pemphigus. *Arch. Dermatol.*, **86**, 493–502.
4. Harris, A., Burge, S.M., Dykes, P.J. and Finlay, A.Y. (1996) Handicap in Darier's disease and Hailey–Hailey disease. *Br. J. Dermatol.*, **135**, 959–963.
5. Heinze, R. (1979) Pemphigus chronicus benignus familiaris (Goujerot-Hailey–Hailey) with affection of mucous membranes. *Dermatol. Monatsschr.*, **165**, 862–867.
6. Kahn, D. and Hutchinson, E. (1974) Oesophageal involvement in familial benign chronic pemphigus. *Arch. Dermatol.*, **109**, 718–719.
7. Botvinick, I. (1973) Familial benign pemphigus with oral mucous membrane lesions. *Cutis*, **12**, 371–373.
8. Václavínkova, V. and Neumann, E. (1982) Vaginal involvement in familial benign chronic pemphigus (Morbus Hailey–Hailey). *Acta Dermatol. Venereol. (Stockh)*, **62**, 80–81.
9. Loewenthal, L. (1959) The role of pyogenic bacteria. *Arch. Dermatol.*, **80**, 318–326.
10. Burns, R.A., Reed, W.B., Swatek, F.E. and Omieczynski, D.T. (1967) Familial benign chronic pemphigus. Induction of lesions by *Candida albicans*. *Arch. Dermatol.*, **96**, 254–258.
11. Richard, G., Linse, R. and Harth, W. (1993) Early detection of genotypical carriers and clinical reliability. *Hautarzt*, **44**, 376–379.

12. Ikeda, S., Suga, Y. and Ogawa, H. (1993) Successful management of Hailey–Hailey disease with potent topical steroid ointment. *J. Dermatol. Sci*., **5**, 205–211.
13. Wilgram, G., Caulfield, J. and Lever, W. (1962) An electronmicroscopic study of acantholysis and dyskeratosis in Hailey–Hailey disease. *J. Invest. Dermatol.*, **39**, 373–381.
14. De Dobbeleer, G., De Graef, C., M'Poudi, E., Gourdain, J.M. and Heenen, M. (1989) Reproduction of the characteristic morphologic changes of familial benign chronic pemphigus in cultures of lesional keratinocytes onto dead deepidermized dermis. *J. J. Am. Acad. Dermatol.*, **21**, 961–965.
15. Regnier, M., Ortonne, J.-P. and Darmon, M. (1990) Histological defects of chronic benign familial pemphigus expressed in tissue culture. *Arch. Dermatol. Res*., **281**, 538–540.
16. Ikeda, S. and Ogawa, H. (1991) Effects of steroid, retinoid and protease inhibitors on the formation of acantholysis induced in organ culture of skins from patients with benign familial chronic pemphigus. *J. Invest. Dermatol.*, **97**, 644–648.
17. Sakuntabhai, A., Ruiz-Perez, V., Carter, S., Jacobsen, N., Burge, S., Monk, S., Smith, M., Munro, C.S., O'Donovan, M., Craddock, N. *et al*. (1999) Mutations in ATP2A2, encoding a Ca^{2+} pump, cause Darier disease. *Nature Genet.*, **21**, 271–277.
18. Ikeda, S., Welsh, E.A., Peluso, A.M., Leyden, W., Duvic, M., Woodley, D.T. and Epstein, E.H.J. (1994) Localization of the gene whose mutations underlie Hailey–Hailey disease to chromosome 3q. *Hum. Mol. Genet.*, **3**, 1147–1150.
19. Richard, G., Korge, B.P., Wright, A.R., Mazzanti, C., Harth, W., Annicchiarico-Petruzzelli, M., Compton, J.G. and Bale, S.J. (1995) Hailey–Hailey disease maps to a 5 cM interval on chromosome 3q21-q24. *J. Invest. Dermatol.*, **105**, 357–360.
20. Peluso, A.M., Bonifas, J.M., Ikeda, S., Hu, Z., Devries, S., Waldman, F., Badura, M., O'Connell, P., Damen, L., Epstein, E. *et al.* (1995) Narrowing of the Hailey–Hailey disease gene region on chromosome 3q and identification of one kindred with a deletion in this region. *Genomics*, **30**, 77–80.
21. Kozak, M. (1987) An analysis of 5′-noncoding sequences from 699 vertebrate messenger RNAs. *Nucleic Acids Res.*, **15**, 8125–8148.
22. Hofman, K., Bucher, P., Falquet, L. and Bairoch, A. (1999) The PROSITE database, its status in 1999. *Nucleic Acids Res.*, **27**, 215–219.
23. Mitchinson, C.M., Wilderspin, A.F., Trinnaman, B.J. and Green, N.M. (1982) Identification of a labelled peptide after stoichiometric reaction of fluorescein isothiocyanate with the Ca^{2+}-dependent adenosine triphosphatase of sarcoplasmic reticulum. *FEBS Lett.*, **146**, 87–92.
24. Ovchinnikov, Y.A., Dzhandzugazyan, K.N., Lutsenko, S.V., Mustayev, A.A. and Modyanov, N.N. (1987) Affinity modification of E1-form of Na^+, K^+-ATPase revealed Asp-710 in the catalytic site. *FEBS Lett.*, **217**, 111–116.
25. Gunteski-Hamblin, A.-M., Clarke, D.M. and Shull, G.E. (1992) Molecular cloning and tissue distribution of alternatively spliced mRNAs encoding possible mammalian homologues of the yeast secretory pathway calcium pump. *Biochemistry*, **31**, 7600–7608.
26. Rudolph, H.K., Antebi, A., Fink, G.R., Buckley, C.M., Dorman, T.E., LeVitre, J., Davidow, L.S., Mao, J.-i. and Moir, D.T. (1989) The yeast secretory pathway is perturbed by mutations in PMR1, a member of a Ca^{2+} ATPase family. *Cell*, **58**, 133–145.
27. MacLennan, D.H., Rice, W.J. and Green, N.M. (1997) The mechanism of Ca^{2+} transport by sarco(endo)plasmic reticulum Ca^{2+}-ATPases. *J. Biol. Chem.*, **272**, 28815–28818.
28. Carafoli, E., Garcia-Martin, E. and Guerini, D. (1996) The plasma membrane calcium pump: recent developments and future perspectives. *Experientia*, **52**, 1091–1100.
29. MacLennan, D.H., Brandl, C.J., Korczak, B. and Green, N.M. (1985) Amino-acid sequence of a Ca^{2+} + Mg^{2+}-dependent ATPase from rabbit muscle sarcoplasmic reticulum, deduced from its complementary sequence. *Nature*, **316**, 696–700.
30. Antebi, A. and Fink, G.R. (1992) The yeast Ca^{2+}-ATPase homologue, PMR1, is required for normal Golgi function and localizes in a novel Golgi-like distribution. *Mol. Biol. Cell*, **3**, 633–654.
31. Sakuntabhai, A., Burge, S., Monk, S. and Hovnanian, A. (1999) Spectrum of novel ATP2A2 mutations in patients with Darier's disease. *Hum. Mol. Genet.*, **8**, 1611–1619.
32. Ruiz-Perez, V.L., Carter, S.A., Healy, E., Todd, C., Rees, J.L., Steijlen, P.M., Carmichael, A.J., Lewis, H.M., Hohl, D., Itin, P. *et al*. (1999) ATP2A2 mutations in Darier's disease: variant cutaneous phenotypes are associated with missense mutations, but neuropsychiatric features are independent of mutation class. *Hum. Mol. Genet.*, **8**, 1621–1630.
33. Hennings, H. and Holbrook, K. (1983) Calcium regulation of cell–cell contact and differentiation of epidermal cells in culture. *Exp. Cell Res.*, **143**, 127–142.
34. Watt, F.M., Mattey, D.L. and Garrod, D.R. (1984) Calcium-induced reorganization of desmosomal components in cultured human keratinocytes. *J. Cell Biol.*, **99**, 2211–2215.
35. Menon, G.K., Grayson, S. and Elias, P.M. (1985) Ionic calcium reservoirs in mammalian epidermis: ultrastructural localization by ion-capture cytochemistry. *J. Invest. Dermatol.*, **84**, 508–512.
36. Pinton, P., Pozzan, T. and Rizzuto, R. (1998) The Golgi apparatus is an inositol, 1, 4, 5-triphosphate-sensitive Ca2+ store, with functional properties distinct from those of the endoplasmic reticulum. *EMBO J.*, **17**, 5298–5308.
37. Munro, S. (1998) Localization of proteins to the Golgi apparatus. *Trends Cell Biol.*, **8**, 11–15.
38. Dürr, G., Strayle, J., Plemper, R., Elbs, S., Klee, S.K., Catty, P., Wolf, D.H. and Rudolph, H.K. (1998) The *medial*-Golgi ion pump Pmr1 supplies the yeast secretory pathway with Ca^{2+} and Mn^{2+} required for glycosylation, sorting, and endoplasmic reticulum-associated protein degradation. *Mol. Biol. Cell*, **9**, 1149–1162.
39. Okorokov, L.A. and Lehle, L. (1998) Ca^{2+}-ATPases of *Saccharomyces cerevisiae*: diversity and possible role in protein sorting. *FEMS Microbiol. Lett.*, **162**, 83–91.
40. Berridge, M.J., Bootman, M.D. and Lipp, P. (1998) Calcium—a life and death signal. *Nature*, **395**, 645–648.
41. Dolmetsch, R.E., Xu, K. and Lewis, R.S. (1998) Calcium oscillations increase the efficiency and specificity of gene expression. *Nature*, **392**, 933–936.
42. Meldolesi, J. (1998) Calcium signalling: oscillations, activation, expression. *Nature*, **392**, 863–866.
43. Riley, J., Butler, R., Ogilvie, D., Finniear, R., Jenner, D., Powell, S., Anand, R., Smith, J.C. and Markham, A.F. (1990) A novel, rapid method for the isolation of terminal sequences from yeast artificial chromosome (YAC) clones. *Nucleic Acids Res.*, **17**, 3425–3433.

MunroeD.J., , Haas, M., Bric, E., Whitton, T., Aburatani, H., Hunter, K., Ward, D. and Housman, D.E. (1994) IRE-Bubble PCR: a rapid method for efficient and representative amplification of human genomic DNA sequences from complex sources. *Genomics*, **19**, 506–514.